



UNIVERSITY OF LEEDS

This is a repository copy of *Observing the impact of Calbuco volcanic aerosols on South Polar ozone depletion in 2015*.

White Rose Research Online URL for this paper:
<http://eprints.whiterose.ac.uk/123544/>

Version: Published Version

Article:

Stone, KA, Solomon, S, Kinnison, DE et al. (13 more authors) (2017) Observing the impact of Calbuco volcanic aerosols on South Polar ozone depletion in 2015. *Journal of Geophysical Research: Atmospheres*, 122 (21). 11,862-11,879. ISSN 2169-897X

<https://doi.org/10.1002/2017JD026987>

Reuse

Items deposited in White Rose Research Online are protected by copyright, with all rights reserved unless indicated otherwise. They may be downloaded and/or printed for private study, or other acts as permitted by national copyright laws. The publisher or other rights holders may allow further reproduction and re-use of the full text version. This is indicated by the licence information on the White Rose Research Online record for the item.

Takedown

If you consider content in White Rose Research Online to be in breach of UK law, please notify us by emailing eprints@whiterose.ac.uk including the URL of the record and the reason for the withdrawal request.



eprints@whiterose.ac.uk
<https://eprints.whiterose.ac.uk/>

RESEARCH ARTICLE

10.1002/2017JD026987

Key Points:

- Ozone-sonde observations show the lowest Antarctic ozone values at 150 hPa since the Pinatubo perturbed years of 1992–1993
- Good agreement between observations and modeling data sets for both ozone changes and the spread of enhanced particle extinction
- Observations suggest that stratospheric volcanic particles from the 2015 eruption of Calbuco greatly enhanced South Polar ozone depletion

Supporting Information:

- Supporting Information S1

Correspondence to:

K. A. Stone,
stonek@mit.edu

Citation:

Stone, K. A., Solomon, S., Kinnison, D. E., Pitts, M. C., Poole, L. R., Mills, M. J., ... Hagiya, S. (2017). Observing the impact of Calbuco volcanic aerosols on South Polar ozone depletion in 2015. *Journal of Geophysical Research Atmospheres*, 122. <https://doi.org/10.1002/2017JD026987>

Received 18 APR 2017

Accepted 9 OCT 2017

Accepted article online 13 OCT 2017

Observing the Impact of Calbuco Volcanic Aerosols on South Polar Ozone Depletion in 2015

Kane A. Stone¹ , Susan Solomon¹ , Doug E. Kinnison² , Michael C. Pitts³, Lamont R. Poole⁴, Michael J. Mills² , Anja Schmidt^{5,6,7} , Ryan R. Neely III^{5,8}, Diane Ivy¹ , Michael J. Schwartz⁹, Jean-Paul Vernier⁴ , Bryan J. Johnson¹⁰ , Matthew B. Tully¹¹, Andrew R. Klekociuk^{12,13} , Gert König-Langlo¹⁴ , and Satoshi Hagiya¹⁵

¹Department of Earth, Atmospheric, and Planetary Science, Massachusetts Institute of Technology, Cambridge, MA, USA, ²Atmospheric Chemistry Observations and Modeling Laboratory, National Center for Atmospheric Research, Boulder, CO, USA, ³NASA Langley Research Center, Hampton, VA, USA, ⁴Science Systems and Applications, Hampton, VA, USA, ⁵School of Earth and Environment, University of Leeds, Leeds, UK, ⁶Department of Chemistry, University of Cambridge, Cambridge, UK, ⁷Department of Geography, University of Cambridge, Cambridge, UK, ⁸National Centre for Atmospheric Science, University of Leeds, Leeds, UK, ⁹Jet Propulsion Laboratory, California Institute of Technology, Pasadena, CA, USA, ¹⁰NOAA/ESRL, Global Monitoring Division, Boulder, CO, USA, ¹¹Bureau of Meteorology, Melbourne, Victoria, Australia, ¹²Australian Antarctic Division, Hobart, Tasmania, Australia, ¹³Antarctic Climate and Ecosystems Cooperative Research Centre, Hobart, Tasmania, Australia, ¹⁴Alfred Wegener Institute for Polar and Marine Research, Bremerhaven, Germany, ¹⁵Meteorological Instrument Center, Japan Meteorological Agency, Tsukuba, Japan

Abstract The Southern Hemisphere Antarctic stratosphere experienced two noteworthy events in 2015: a significant injection of sulfur from the Calbuco volcanic eruption in Chile in April and a record-large Antarctic ozone hole in October and November. Here we quantify Calbuco's influence on stratospheric ozone depletion in austral spring 2015 using observations and an Earth system model. We analyze ozonesondes, as well as data from the Microwave Limb Sounder. We employ the Community Earth System Model, version 1, with the Whole Atmosphere Community Climate Model (WACCM) in a specified dynamics setup, which includes calculations of volcanic effects. The Cloud-Aerosol Lidar with Orthogonal Polarization data indicate enhanced volcanic liquid sulfate 532 nm backscatter values as far poleward as 68°S during October and November (in broad agreement with WACCM). Comparison of the location of the enhanced aerosols to ozone data supports the view that aerosols played a major role in increasing the ozone hole size, especially at pressure levels between 150 and 100 hPa. Ozonesonde vertical ozone profiles from the sites of Syowa, South Pole, and Neumayer display the lowest individual October or November measurements at 150 hPa since the 1991 Mount Pinatubo eruption period, with Davis showing similarly low values, but no available 1990 data. The analysis suggests that under the cold conditions ideal for ozone depletion, stratospheric volcanic aerosol particles from the moderate-magnitude eruption of Calbuco in 2015 greatly enhanced austral ozone depletion, particularly at 55–68°S, where liquid binary sulfate aerosols have a large influence on ozone concentrations.

1. Introduction

Volcanic sulfur aerosols can have significant influences on stratospheric ozone concentrations by enhancing surface areas for heterogeneous chemistry (Hofmann & Solomon, 1989; Portmann et al., 1996), including in high southern latitudes during austral spring, when large ozone depletion occurs. In 2015 the Southern Hemisphere stratosphere experienced both an injection of 0.4 Tg of SO₂ from the 23 April moderate-magnitude volcanic eruption of Calbuco, followed by record Antarctic ozone loss in October (Solomon et al., 2016). Here we present a broad range of observations, complemented by model simulations, to examine and characterize the impact of the 2015 Calbuco eruption on stratospheric ozone.

Recently, austral spring column ozone over Antarctica is routinely reduced by ~50% compared to pre-1979 levels, creating the Antarctic ozone “hole” (Solomon, 1999). This depletion was identified by Chubachi (1985) and Farman et al. (1985), and first explained by Solomon et al. (1986). The formation of the ozone hole results from the combination of anthropogenic emissions of ozone-depleting substances (ODSs), mainly in the form of chlorofluorocarbons, and the dynamical conditions of the Southern Hemisphere (see references in the review by Solomon (1999)). The chlorine from ODSs is generally tied up in the

inactive ozone reservoir species HCl and ClONO₂, but these react on the surfaces of Antarctic polar stratospheric clouds (PSCs) or aerosols under very cold conditions to produce much more reactive forms of chlorine. The reactive chlorine then catalytically destroys ozone when sunlight returns in the spring. Considering that the amount of chlorine and other ODSs (such as bromine) is rather stable in the stratosphere, the year-to-year variability in the size of the ozone hole is generally driven by differing dynamical conditions. For example, a colder, more stable Southern Hemisphere stratosphere will result in more ideal conditions for ozone loss since the reactivity on the surfaces of PSCs is heavily dependent on small perturbations in temperature (see Solomon et al., 2015). However, another important factor is the amount of sulfur in the stratosphere, which can modify some PSCs and enhance the number concentrations of reactive binary liquid sulfuric acid aerosols.

The existence of a background sulfur aerosol layer has long been known (Junge et al., 1961). Major sources include transport of surface emissions of SO₂, dimethyl sulfide, and carbonyl sulfide to the stratosphere, which oxidize to form H₂SO₄, and then condenses to liquid binary sulfate (LBS) aerosol of H₂SO₄-H₂O (Brock et al., 1995; Kremser et al., 2016). More recently, the variable nature of the stratospheric aerosol layer due to episodic volcanic sources of sulfur has been shown (Solomon et al., 2011; Vernier et al., 2011). The presence of LBS plays many important roles in stratospheric chemistry and has been studied extensively (e.g., Cox et al., 1994; Portmann et al., 1996; Solomon et al., 1998; Tilmes et al., 2008). In the polar regions, as temperatures begin to approach the frost point, LBS will take up HNO₃ and become liquid supercooled ternary solutions (STSs) of HNO₃-H₂SO₄-H₂O (Molina et al., 1993). Type Ib PSCs, composed of STS, can coexist with type Ia frozen nitric acid trihydrate (NAT) particles (Pitts et al., 2013; Pitts, Poole, & Thomason, 2009). Enhanced volcanic sulfur loading in the stratosphere will typically lead to an increase in LBS aerosols at all latitudes in the lower stratosphere, and can enhance ozone loss dramatically in the polar regions (Portmann et al., 1996), and to a lesser extent outside of the polar vortex (Hanson et al., 1994; Solomon et al., 1996). The heterogeneous reactivity of LBS aerosols is strongly dependent on temperature, with colder temperatures allowing more uptake of water causing the LBS particles to swell (Solomon, 1999, and references therein). At greater pressure, effective heterogeneous reactions are able to take place under volcanic conditions at higher temperatures where PSCs seldom form (Hofmann & Oltmans, 1993).

If an eruption is located in the tropics or Southern Hemisphere, the aerosols can be transported to the South Pole through the general circulation of the stratosphere (see Butchart, 2014, and references therein). This was observed after the 15 June 1991 eruption of Mount Pinatubo (15.13°N, 120.35°E), which injected 14–23 Tg of SO₂ into the stratosphere (Guo et al., 2004). In combination with influence from the smaller Cerro Hudson volcanic eruption, over the next 2–3 years, anomalous ozone depletion was recorded due to enhanced sulfate levels over the South Pole during the austral spring (Bluth et al., 1992; Brasseur & Granier, 1992; Hofmann et al., 1992; Hofmann & Oltmans, 1993; Rosenfield et al., 1997; Rozanov et al., 2002), especially at pressures greater than 100 hPa (Hofmann et al., 1997; Solomon et al., 2005). The heating of the stratosphere caused by excess volcanic aerosols may also modulate the transport of ozone southward. This was seen after Pinatubo, where stratospheric heating due to excess aerosols strengthened the Brewer-Dobson circulation, transporting more ozone toward the southern midlatitudes during the winter of 1991 (Aquila et al., 2013; Poberaj, Staehelin, & Brunner, 2011).

On 23 April 2015, the Chilean volcano, Calbuco (41.33°S, 287.39°E), erupted (Castruccio et al., 2016; Romero et al., 2016). This eruption injected an estimated 0.4 Tg of SO₂ into the stratosphere up to an altitude of 20–21 km (Nicarnica Aviation, 2015; Pardini et al., 2017; Solomon et al., 2016). Although Calbuco injected far less SO₂ into the stratosphere in 2015 than Pinatubo did in 1991, its closer proximity may have allowed transport of a larger fraction of its sulfate aerosol to the Antarctic.

Ivy et al. (2017), using a free running chemistry-climate model, showed that Calbuco aerosols played a key role in 2015 ozone depletion. However, loss similar to that of the specified dynamics run that was nudged to the Modern-Era Retrospective Analysis for Research and Applications (MERRA) reanalysis dynamical fields (Rienecker et al., 2011) was only seen in free running simulations with anomalously low temperatures. The 2015 Antarctic spring lower stratosphere was, indeed, abnormally cold, and these low temperatures likely contributed significantly to anomalous ozone depletion (WMO, 2015). Here observational data sets are used in combination with modeling data sets to analyze the observational evidence for the spread of Calbuco sulfate aerosols and the extent of volcanic contribution to South Polar ozone depletion in 2015.

2. Model Description

The model used in this study is the Community Earth System Model, version 1 (CESM1) (Marsh et al., 2013), a fully coupled climate model featuring four separate modules for simulating the atmosphere, ocean, land surface, and sea ice. The atmospheric portion of CESM1 used here is the Whole Atmosphere Community Climate Model, version 4 (WACCM4), executed in specified dynamics mode using fields of temperature, zonal wind, meridional wind, and surface pressure nudged to MERRA. A horizontal resolution of 1.9° latitude by 2.5° longitude and 88 vertical levels with a high top at 5.1×10^{-6} hPa (~140 km) are used in the specified dynamics version.

The chemical scheme used is based on the Model of Ozone and Related Tracers (Kinnison et al., 2007) and includes 183 different species, 341 gas phase reactions, 114 photolytic processes, and 17 heterogeneous reactions on multiple aerosol types. This includes the O_x , NO_x , HO_x , ClO_x , and BrO_x chemical families, heterogeneous reactions on liquid binary and ternary sulfate polar stratospheric cloud (PSC) particles, and solid nitric acid trihydrate and water ice PSCs. This model setup has been shown to simulate Antarctic ozone depletion and levels of chlorine reservoir species accurately (Solomon et al., 2015). The simulation of PSCs in the model maintains both liquid and solid particles under very cold conditions (Wegner et al., 2013). LBS is the only aerosol represented at temperatures above ~200 K.

Sulfate aerosols are represented following calculations from the three-mode version of the Modal Aerosol Model version 3 (MAM3), presented in Mills et al. (2016). This contains an inclusive time series of sulfur dioxide (SO_2) emissions and plume altitudes from all known stratospheric volcanic sources (see Mills et al. (2016) for details of the implementation of the VolcanEESM database created by Neely and Schmidt (2016)), as well as natural and anthropogenic background sources of SO_2 . The three modes of Aitken, accumulation, and coarse are simulated by MAM3, and these distributions evolve through nucleation, condensation, coagulation, and sedimentation processes. This gives a comprehensive characterization of sulfur aerosols, and comparisons of MAM3 and observations were presented in Mills et al. (2016).

Using the setup described above, two simulations over the time period of 1999–2015 are compared to observations to investigate the influence of volcanic aerosols on ozone: (1) a simulation with full representation of sulfur aerosols as described above (henceforth, labeled MAM) and (2) a simulation using only background sources of SO_2 (volcanically clean, henceforth labeled VC-MAM). This, in combination with specified dynamics, allows isolation of the chemical impact of volcanic aerosols on ozone under the same dynamical conditions that occurred in 2015. This means that VC-MAM will also include any aerosol-induced temperature feedback and therefore does not allow analysis of the dynamical and thermal responses. However, Iry et al. (2017) showed through analysis of the key species in ozone depletion that the dynamical/thermal feedback were less important to the ozone loss than the aerosol-induced chemical response.

3. Observational Data Sets

3.1. Ozonesondes

Ozonesonde measurements from the four Antarctic sites of South Pole (90°S), Neumayer (70.7°S, 351.7°E), Syowa (69°S, 39.6°E), and Davis (68.6°S, 78°E) are used in this analysis. All measurements were performed with an electrochemical cell ozonesonde and followed the manufacturer chemical concentration recommendations (Deshler et al., 2008; Deshler et al., 2017), except at Syowa before March 2010, where a carbon-iodide cell was used. Both laboratory and atmospheric comparisons of ozonesondes with a UV spectrometer report a precision (comparison of average ozonesonde standard deviations relative to the UV spectrometer) of 3–5% and an accuracy (bias + precision) of 5–10% in the stratosphere (Deshler et al., 2008; Smit et al., 2007).

3.2. Microwave Limb Sounder

The Microwave Limb Sounder (MLS) instrument on board the Aura satellite is used to evaluate ozone over the Antarctic and Southern midlatitude regions at the two pressure levels of 146.8 and 100 hPa (Livesey et al., 2016). The Aura satellite orbits in a Sun-synchronous orbit covering latitudes 81.1°S–81.8°N and MLS has produced ~3500 suborbital ozone profiles per day from 2004 to present. Version 4 data shown here have been screened based on quality control described in Livesey et al. (2016). At 146.8 and 100 hPa, MLS ozone data have a precision of ~20 ppbv and ~30 ppbv, respectively, and a vertical resolution of 3 km. Comparison with other observational data sets shows agreement to 5–10% (Livesey et al., 2016).

3.3. Cloud-Aerosol Lidar With Orthogonal Polarization

The Cloud-Aerosol Lidar with Orthogonal Polarization (CALIOP) instrument on board the Cloud-Aerosol Lidar and Infrared Pathfinder Satellite Observation (CALIPSO) is used to compare level 1B v4.10 532 nm zonal mean-attenuated particulate backscatter to MAM and VC-MAM extinction coefficients during 2015. The data are averaged in 2° latitude bins and have an approximate 180 m vertical resolution. We use data from May to November 2015 (Winker et al., 2009). Rogers et al. (2011) showed CALIOP level 1B 532 nm total attenuated backscatter data to be accurate to within 3% when compared to internally calibrated measurements from an airborne high spectral resolution lidar during a series of 86 CALIPSO underflights. Assuming additional uncertainty in molecular number density, CALIOP-attenuated particulate backscatter data used herein are estimated to be accurate to within 4–5%. For the zonal mean data used here, each 2° latitude by 180 m altitude bin has a relative zonal standard deviation that is on average about 10–20% of mean.

3.4. Ozone Monitoring Instrument

The Ozone Monitoring Instrument (OMI) on board the Aura satellite is used to evaluate South Polar total column ozone (TCO) (Levelt et al., 2006). The instrument is an ultraviolet/visible nadir-viewing solar backscatter spectrometer, and the data set spans the temporal range of 2004 to present. We use the level 3 data product which is globally gridded to 1° latitude by 1° longitude. The OMI level 3 data have an uncertainty similar to that of the Total Ozone Mapping Spectrometer (TOMS) and thus have a root-mean-square error of around 2% (Levelt et al., 2006). Comparison of TOMS with ground-based instruments showed agreement at around 1% (McPeters et al., 1998).

4. Results

4.1. Southward Dispersal of Calbuco Aerosols

Figure 1 shows the temporal and spatial evolution of the Calbuco liquid binary volcanic sulfate aerosols as seen by both the CALIOP satellite and the MAM simulation. The MAM 550 nm extinction data are divided by an adopted extinction to backscatter ratio of 50 for comparison to CALIOP 532 nm backscatter observations (Jäger & Deshler, 2002, 2003). The data are also scaled appropriately to account for the slightly different wavelengths. It is important to note that the extinction to backscatter ratio used is an estimation only. The scale factor may not be the same for different altitudes if, for example, particle sizes are dependent on height, introducing possible differences. The monthly average MAM values also do not use coincident CALIOP measurement times, which could introduce some biases in absolute values. Nevertheless, this comparison does demonstrate where the aerosols are residing in the data versus the model. Values at pressure levels of 100 hPa and 146.8 hPa are shown from May to November and over the latitude range of 90–32°S. These pressure levels are displayed here due to sulfur aerosol tendency to influence ozone concentrations at pressures greater than 100 hPa (Solomon, 1999), as discussed further below. A pressure-latitude comparison is also shown for the month of August. Our focus here is the spread of the volcanic aerosols, rather than the challenging task of estimating how volcanic material may influence ice and NAT PSCs. The presence of ice and STS PSCs is therefore masked from the CALIOP backscatter and model aerosol extinction data using WACCM STS PSCs and ice definitions. We define STS or NAT PSCs to be present when the ratio of simulated condensed HNO₃ to gas phase HNO₃ is greater than 0.1, and we filter areas where ice clouds occur in the model. What remains are the areas where the LBS component is present independently of STS and ice. We also mask the CALIOP data below 150 hPa to remove any significant influence from high tropospheric clouds.

At 100 hPa and 146.8 hPa, CALIOP shows the southward progression of sulfur from its stratospheric injection in April. The peaks in June and August at 100 hPa and in September and October at 146.8 hPa mark the times when the descent of the majority of the aerosols reached these pressure levels. Large values persist until November as far as 68°S, while the descent of the aerosols continues through November, as seen in Figure S1 in the supporting information. MAM extinction values are slightly larger than CALIOP (by about 10% on average), possibly a result of the scaling factor used. However, the timing of the southward progression is captured very well by MAM as compared to CALIOP at these pressure levels. Further, the latitude-pressure plot for the month of August (and Figure S1) also shows that MAM's distribution of aerosols in the vertical generally agrees very well with CALIOP.

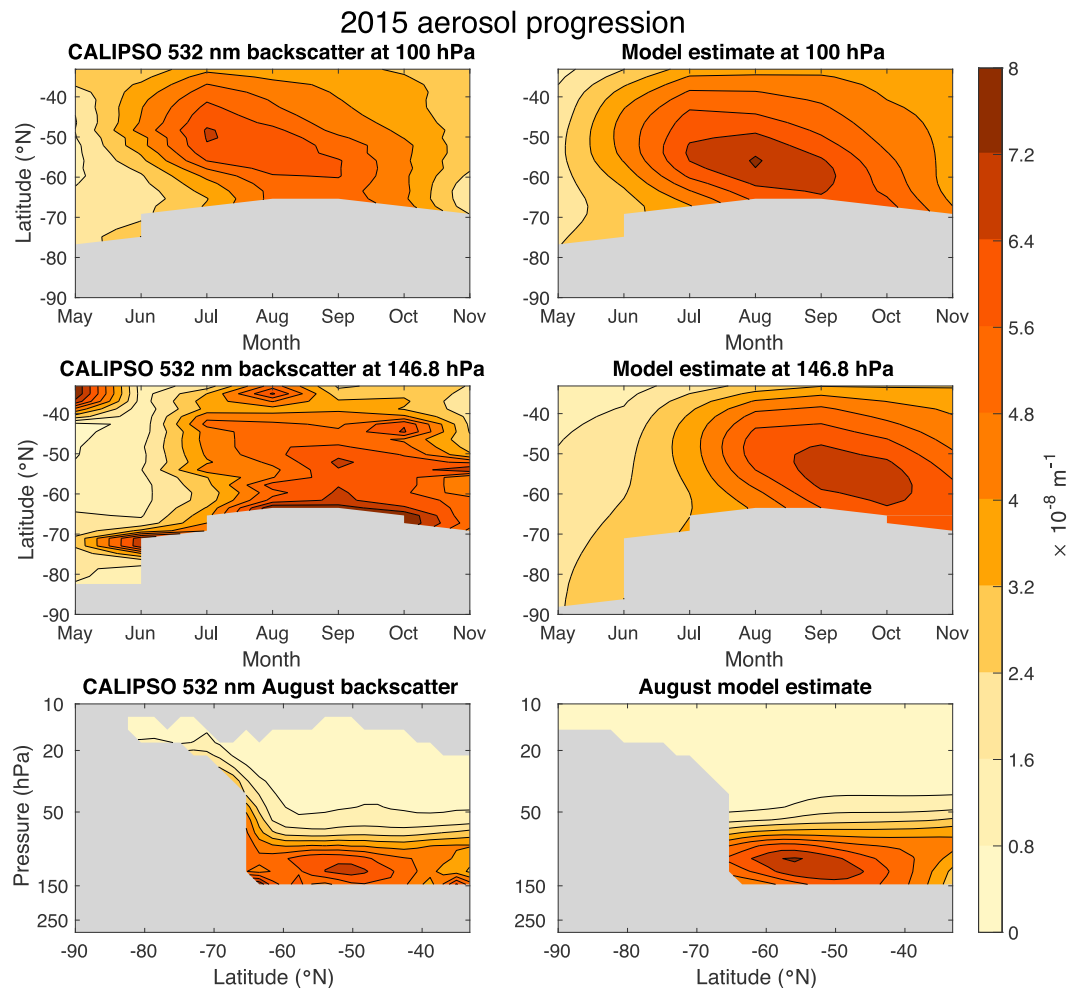


Figure 1. Progression of Calbuco volcanic aerosols from May to November 2015 at 100 and 146.8 hPa inferred from CALIOP backscatter at 532 nm as compared to MAM 550 nm extinction (see text). The extinction values are divided by an extinction to backscatter ratio of 50. August latitude-pressure plots of the extinction inferred from CALIOP and that in the model are also shown.

As mentioned previously, the location of the Calbuco volcano compared to Pinatubo will have likely allowed a higher-percentage transport of aerosol particles southward. We investigate this further in Figure 2, where model-derived aerosol surface area densities (SADs) for chemistry for the Pinatubo years of 1991–1993 and the Calbuco year of 2015 are shown for 60°S and at 100 hPa. It is seen that in 1991, the year that Pinatubo erupted, SAD levels in the key month of September were about 2 to 3 times those obtained after Calbuco in 2015. Over the following 2 years, they decreased but still remained elevated. However, even though the Calbuco eruption injected considerably less total sulfur into the stratosphere than Pinatubo, the Calbuco 2015 SAD levels at 60°S and 100 hPa are of similar magnitude to 1992 and 1993 from August to October. It is also seen that the 2015 Calbuco SAD decreases rapidly after September, similar to Pinatubo in 1991.

Considering that there are largely observed aerosol extinctions as far as 68°S, and that the amount of sulfur simulated by the model is of comparable magnitude to the well-documented Pinatubo event, LBS could have acted as a significant surface for heterogeneous chemistry equatorward of 68°S. At 146.8 hPa there is an increase in extinction near 68°S in the CALIOP data. This is likely due to when moving further poleward, the LBS particles swell, making it difficult to separate what is transported LBS and what is PSC. Also, small-temperature errors in MERRA make it difficult to know the amount of additional temperature-dependent LBS that is present in the model. Therefore, analysis of when and how much volcanic LBS entered the

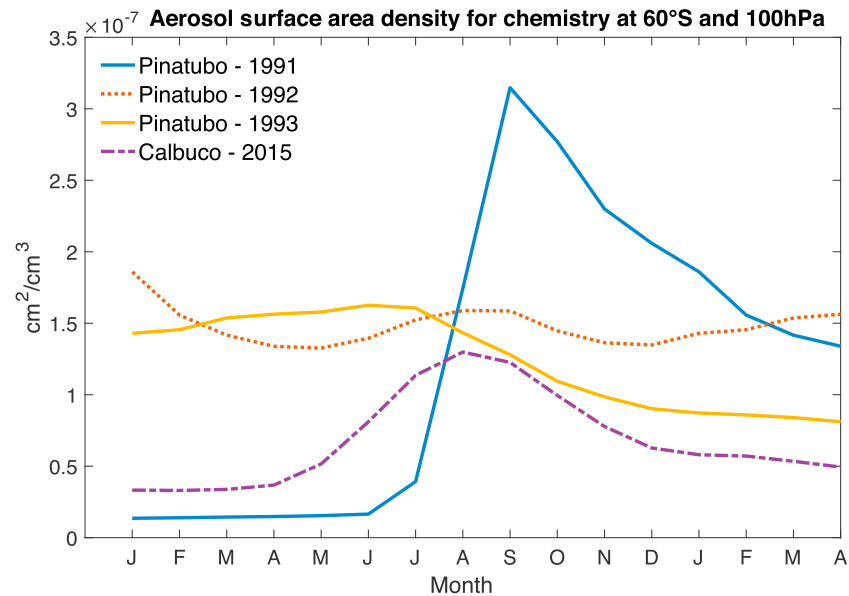


Figure 2. Aerosol surface area density for chemistry as derived by MAM at 60°S and 100 hPa for the Pinatubo years 1991–1993 and the Calbuco year 2015.

polar is not analyzed in this paper. However, below we will show that the edge region of the polar vortex (which not usually experience as much ozone depletion as higher latitudes) provides a key location to detect the influence of volcanic aerosols on ozone depletion, using a comparison of the MAM and VC-MAM simulations with observations.

4.2. Normalized Ozone Anomalies

In order to compare MAM and VC-MAM anomalies with MLS and OMI observations over the available MLS period of 2004–2015, normalized ozone anomalies are calculated. Normalized zonal and monthly mean anomalies were constructed by subtracting the 2004–2015 monthly climatology from each corresponding month, which was then divided by their associated 2004–2015 monthly standard deviations. This gives all time series a mean of 0 and a standard deviation of 1 and accounts for biases between MAM, VC-MAM, and MLS. Figure 3 shows time-latitude normalized ozone anomalies at 100 hPa for MLS, MAM, and VC-MAM, and TCO for OMI, MAM, and VC-MAM from May to December 2015.

The MLS normalized 2015 anomalies at 100 hPa show large negative ozone anomalies, less than -1.5 , over the entire ozone hole period of September through December as far north as 45°S, and as far south as 82.5°S, especially during October and November. The lowest ozone anomalies occur during October between approximately 55 and 70°S, with values less than -2.25 . The MAM simulation shows very good agreement at 100 hPa (with only slightly larger normalized anomalies seen in the MAM simulation). The MAM simulation also shows normalized anomalies less than -1.5 as far north as 45°S. The VC-MAM simulation does show negative normalized anomalies, but not to the same extent as MAM or MLS, with values not lower than -1.75 anywhere, suggesting that aerosols are having an influence on ozone depletion at 100 hPa. Also, normalized anomalies extend up to 50 hPa in MLS and MAM that are larger compared to VC-MAM (see Figure S3), suggesting that volcanic aerosols also played a role at smaller pressures.

The OMI TCO normalized anomalies look similar to what is seen by MLS at 100 hPa. The largest anomalies, less than -2 , are seen during October between 60 and 70°S. A very similar structure is seen in the MAM simulation, with the largest normalized anomalies, again less than -2 , occurring in the same region as what is seen in OMI. However, MAM does show somewhat larger normalized anomalies everywhere compared to OMI. Further, contrary to 100 hPa, VC-MAM shows relatively large normalized anomalies for some months as well, albeit smaller than those in the OMI data.

The positive normalized anomalies that occur in all data sets, but more pronounced in MLS, before the ozone hole period suggest excess ozone transport southward, perhaps implying a similar mechanism as to what

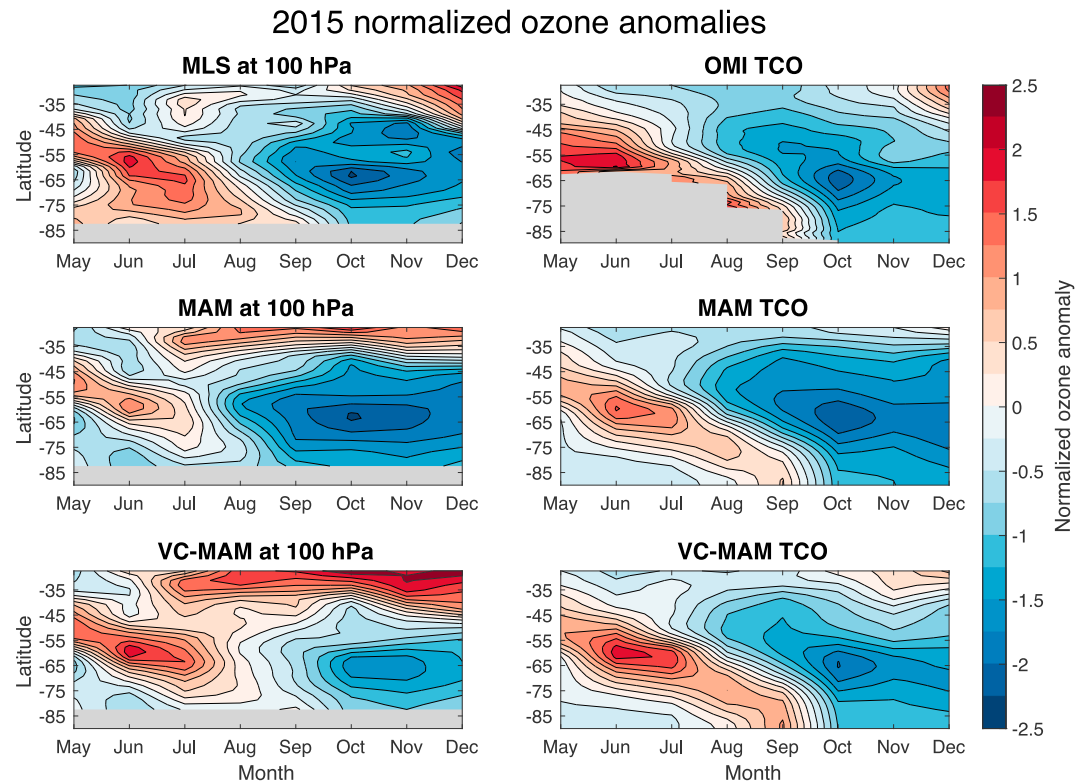


Figure 3. The 2015 normalized ozone anomalies from the 2004–2015 MLS, MAM, and VC-MAM time series shown as zonally averaged time-latitude maps (see text).

occurred in 1991, where heating due to aerosols played a role in enhancing the Brewer-Dobson circulation and thus southward transport (Aquila et al., 2013; Poberaj et al., 2011).

Figure 4 shows absolute differences and percent differences from VC-MAM for the MAM and VC-MAM simulations from May to December 2015. This compliments Figure 3 nicely, showing the largest simulated difference in ozone number density at 100 hPa and TCO during September and October near 65°S of up to 1×10^{12} molecules per cm^3 and 20 Dobson units (DU), respectively. The largest percent changes occur a little later in the year during October and November, and extent as far as 90°S in TCO, with differences as large as 10%. The percent differences in number density at 100 hPa are much larger, as high as 80% during October between 70 and 80°S. It is also interesting to note that the volcanic influence in the model is extending as far north as 32°S with 1–2% changes occurring in TCO from June to December, and up to 16% occurring at 100 hPa from August to December.

The presence of aerosols in Figure 1 and the large negative normalized anomalies seen in MLS at 100 hPa in Figure 3 suggest that aerosols are likely to be a key driver of the anomalous ozone depletion in this region. This is supported by the large difference in the normalized anomalies between MAM and VC-MAM at 100 hPa, and the large absolute and percent differences between MAM and VC-MAM seen in Figure 4. However, the smaller anomalies that are still present in VC-MAM highlight that the anomalously cold temperatures of 2015 also contribute (see Figure S2) (Ivy et al., 2017). Approaching the South Pole, the temperatures are typically very cold, and near-complete ozone destruction often occurs (especially between 100 hPa and 50 hPa, but also sometimes at greater pressure), implying saturation. This makes it likely that the largest volcanic ozone depletion anomalies will occur at lower less saturated latitudes, especially under ideal dynamical conditions. Since the region between 60 and 75°S is generally on the edge or outside the polar vortex, excess ozone depletion in this region should act to expand the size of the ozone hole. Further analysis of the expansion of the ozone hole during 2015 compared to recent climatology is shown in the next section.

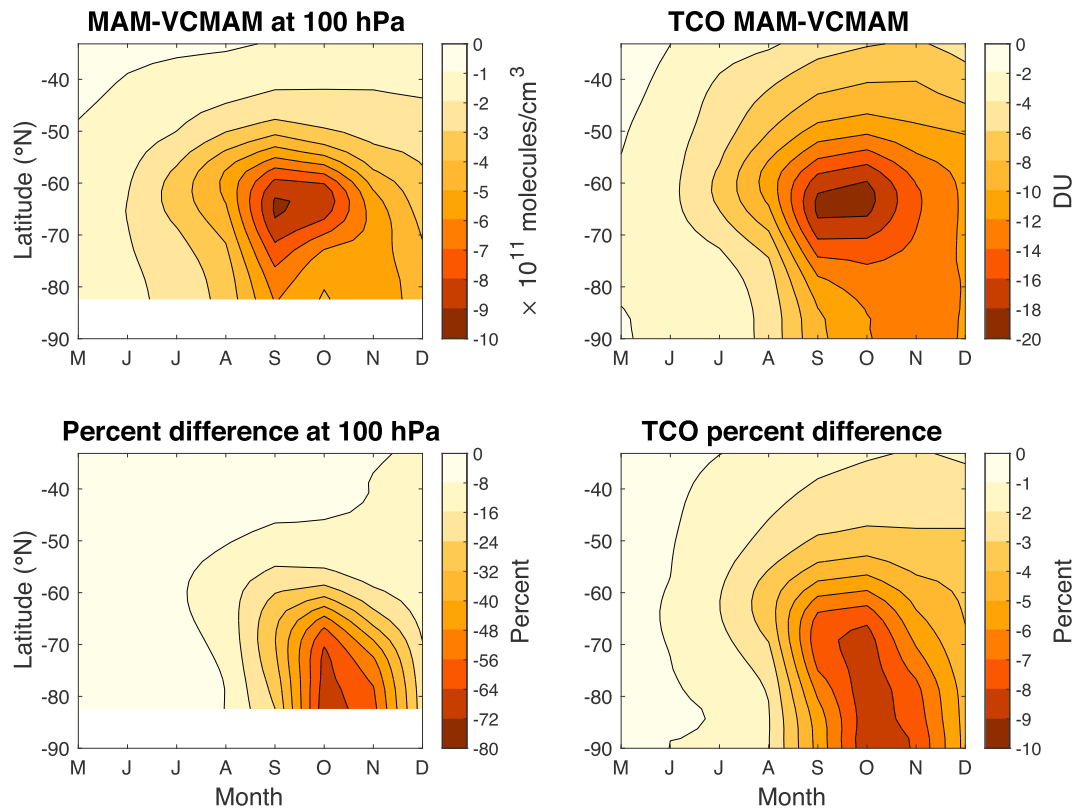


Figure 4. MAM minus VC-MAM absolute and percent differences for May to December 2015.

4.3. Latitudinal Expansion of the Ozone Hole

Figure 5 shows the TCO contour line values of the ozone hole as seen in WACCM and OMI based on the standard definition of 220 DU (Newman, Kawa, & Nash, 2004). Contours delineating averaged values below 0.275 ppmv are also shown at 100 and 150 hPa. Since the 2015 values are so low compared to climatology, the value of 0.275 ppmv was chosen, as it is contained within the high ozone gradient region for 2015 based on the model, but is very low compared to climatology. The locations of the ozonesonde stations, Davis, Syowa, and Neumayer, are also shown. This analysis does not describe the amount of depletion, just the size of the area where ozone is below the given thresholds.

In the TCO plots for September and October 2015, the MAM simulation agrees very well with OMI, with only a slightly larger 220 DU contour boundary in OMI during September. The VC-MAM 220 DU contour boundary is smaller over all longitudes, with the difference in area between MAM and VC-MAM calculated to be a substantial 4.4 (approximately 24%) and 3.5×10^6 km² (approximately 17%) during September and October, respectively (see Solomon et al., 2016). Comparison of MAM, VC-MAM, and OMI for 2015 with the 2004–2014 OMI average shows that the majority of the expansion of the ozone hole occurred between 90 and 180°E during September and between 90 and 270°E during October. This is especially the case during October, and is in the opposite region of the continent relative to where the ozone hole is typically centered, as seen in the climatology. Therefore, the cold, stable dynamical conditions, as seen in VC-MAM and Figure S2, have made the ozone hole more symmetrical about the geographic South Pole. Importantly, Figure 5 shows that the extent of the increase in the ozone hole area during September and October cannot be explained in the model without the inclusion of the Calbuco volcanic aerosols.

For November 2015 there is again very good agreement between MAM and OMI. The average ozone hole is much smaller than October and September. The lower temperatures and stability of the vortex in November 2015 have allowed the ozone hole to expand along all longitudes. Volcanic aerosols result in a larger ozone hole by 2.8×10^6 km² in the model (approximately 16%).

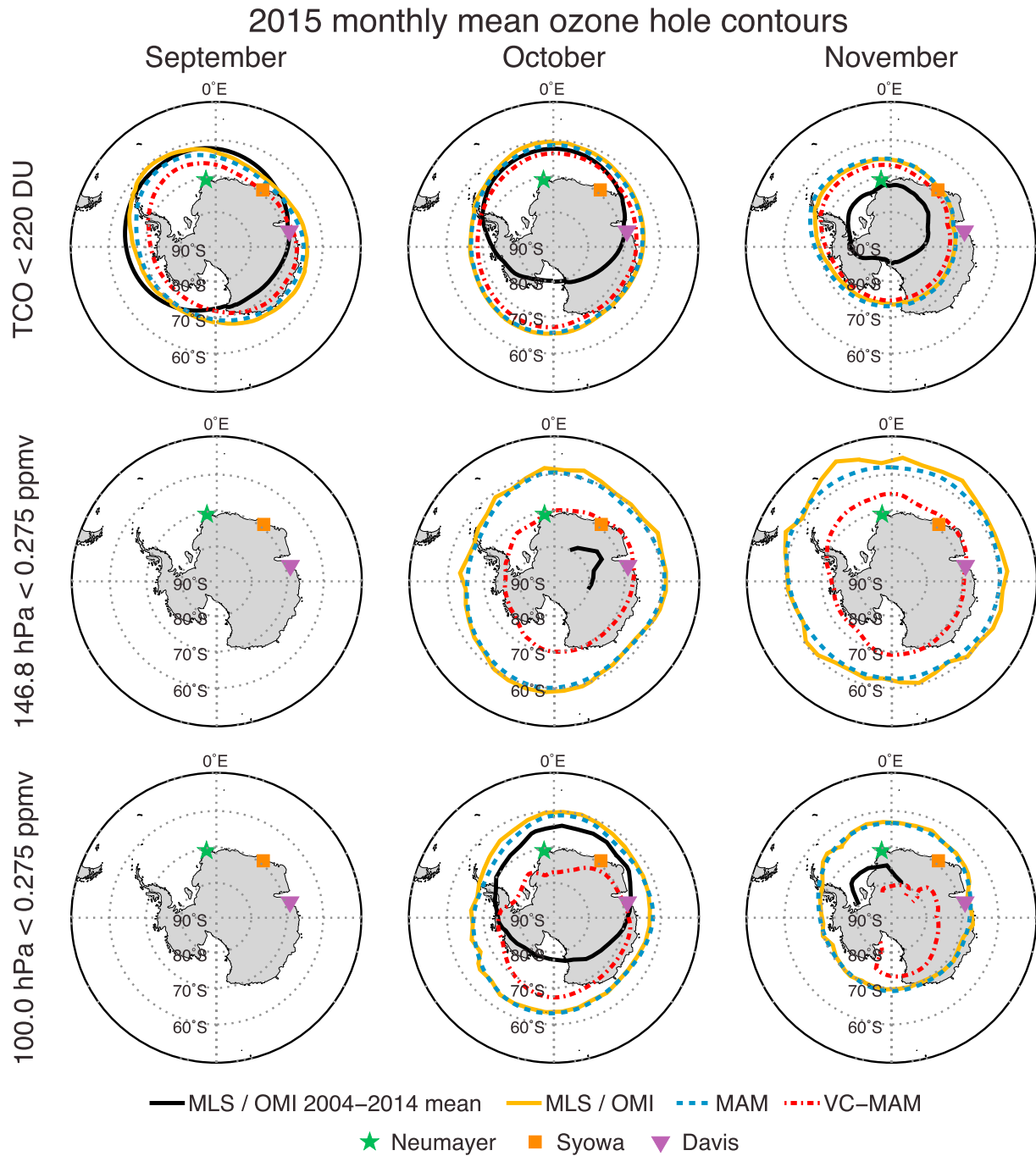


Figure 5. TCO 220 DU contour for OMI, MAM, and VC-MAM and the 0.275 ppmv contour at 146.8 and 100 hPa for MLS, MAM, and VC-MAM. The ozone sonde stations Neumayer, Syowa, and Davis are shown as symbols.

We next compare MLS data at 150 and 100 hPa levels to the model. During September in 2015, there are no observed monthly average values below the 0.275 ppmv value, while during October and November, the 0.275 ppmv contour lines are seen at 60–70°S. This is in contrast to what is seen in TCO, where September and October show the largest ozone holes. This is consistent with the altitude dependence of the timing of ozone depletion, where low ozone values persist later in the year at greater pressure (Solomon et al., 2005). However, it could also be influenced by the timing of volcanic aerosol descent, as seen in Figure 1. In October and November, the areas enclosed by the MLS and MAM 0.275 ppmv contours become very

large and quite consistent with one another at both 100 hPa and 150 hPa. The difference between MAM and VC-MAM is much larger compared to the TCO case, consistent with Figures 3 and 4. In addition, there are almost no November values from the MLS 2000–2014 average at either 100 hPa or 150 hPa that are below the 0.275 ppmv level, highlighting the unusual extent of ozone depletion during 2015. The contrast between the 2015 MAM and MLS values, the MLS 2004–2014 average, and 2015 VC-MAM highlights the significant influence that volcanic aerosols had at these greater pressure levels.

The likely reason that the expansion of the ozone hole is much greater at larger pressure levels compared to TCO is that while ozone between 100 and 50 hPa is the most significant contributor to the TCO metric outside of the ozone hole season, it is also the location where ozone depletion is often nearly saturated, at close to total ozone loss. Ozone does not typically deplete to the same extent at greater pressure levels where temperatures are too warm for PSCs, as shown in the next section, meaning that volcanic aerosols, when they are present under the right conditions, have a larger influence on the expansion of ozone depletion at pressures greater than 100 hPa. This also agrees with the difference in normalized anomalies in TCO and at 100 hPa between MAM and VC-MAM in Figure 3.

The locations of the ozonesonde stations as shown in Figure 5 are key for comparisons of the ozonesonde measurements to MAM and VC-MAM simulations that are presented below. Due to the dynamical nature of the polar vortex, these lower latitude stations may sample air that is both inside and outside of the polar vortex in a given month. Looking at the OMI TCO data (Figure 5) suggest that this should be expected at Davis in particular, a point discussed below.

4.4. Ozone Vertical Profiles

The previous sections showed that large negative ozone anomalies occurred in 2015 in MLS and OMI observations from about 50 to 70°S, depending upon month. Comparison with MAM and VC-MAM simulations suggests that Calbuco sulfur aerosols have played a large role in this depletion. We now turn to the higher vertical resolution information that is available from Antarctic ozonesonde stations. Figure 6 compares October ozonesonde measurements of the well-documented, Pinatubo-induced low ozone events of 1992 and 1993, to 2015, and the more volcanically quiet periods of 1996–2000 and 2012–2014. October averages are shown for the sites of South Pole, Neumayer, Syowa, and Davis. Since the time series at Davis starts in 2004, only the 2012–2014 and 2015 periods are compared.

At the South Pole, Neumayer, and Syowa there are large differences between the volcanically clean eras of 1996–2000 and 2012–2014, with the 2012–2014 period showing larger ozone values due to healing as ODSs are reduced (Solomon et al., 2016).

During the 1992–1993 post-Pinatubo years at South Pole, Neumayer, and Syowa, the amount of ozone at pressures less than 100 hPa is similar or even larger compared to the more volcanically clean periods. However, at greater pressures from about 100 to 200 hPa, the post-Pinatubo years show significantly less ozone. As mentioned previously, this is the region where volcanic aerosols are expected to have the largest effect.

During 2015, a large negative anomaly compared to the two volcanically clean periods is seen at pressures greater than 100 hPa at all four stations, with a structure similar to 1992–1993 at the three stations where data exist for that period. MAM also shows a large negative anomaly during 2015 when compared to 2012–2014 (see Figure S4). The similarity of the ozone profile shapes in 1992–1993 and 2015 supports the view that volcanic aerosols had an influence during both periods at these pressure levels. There was also a significant amount of depletion at pressures less than 100 hPa in 2015 compared to 2012–2014 due to the unusually cold conditions that occurred during 2015. Thus, the low TCO conditions during 2015 are likely a combination of the dynamical conditions and excess volcanic aerosols. In the next section, individual ozonesonde ozone measurements are shown and compared to MLS and MAM for all data over the 1990–2015 period.

4.5. Ozone Time Series at 150 hPa

Figures 7 and 8 show October and November ozone time series at 150 hPa for the four ozonesonde locations listed in section 3.1. This pressure level typically displays less variability compared to smaller pressures, making it easier to separate the volcanic effects when looking at individual measurements. Two observational data sets, ozonesondes and MLS, are compared to MAM and VC-MAM calculations. The MLS observations

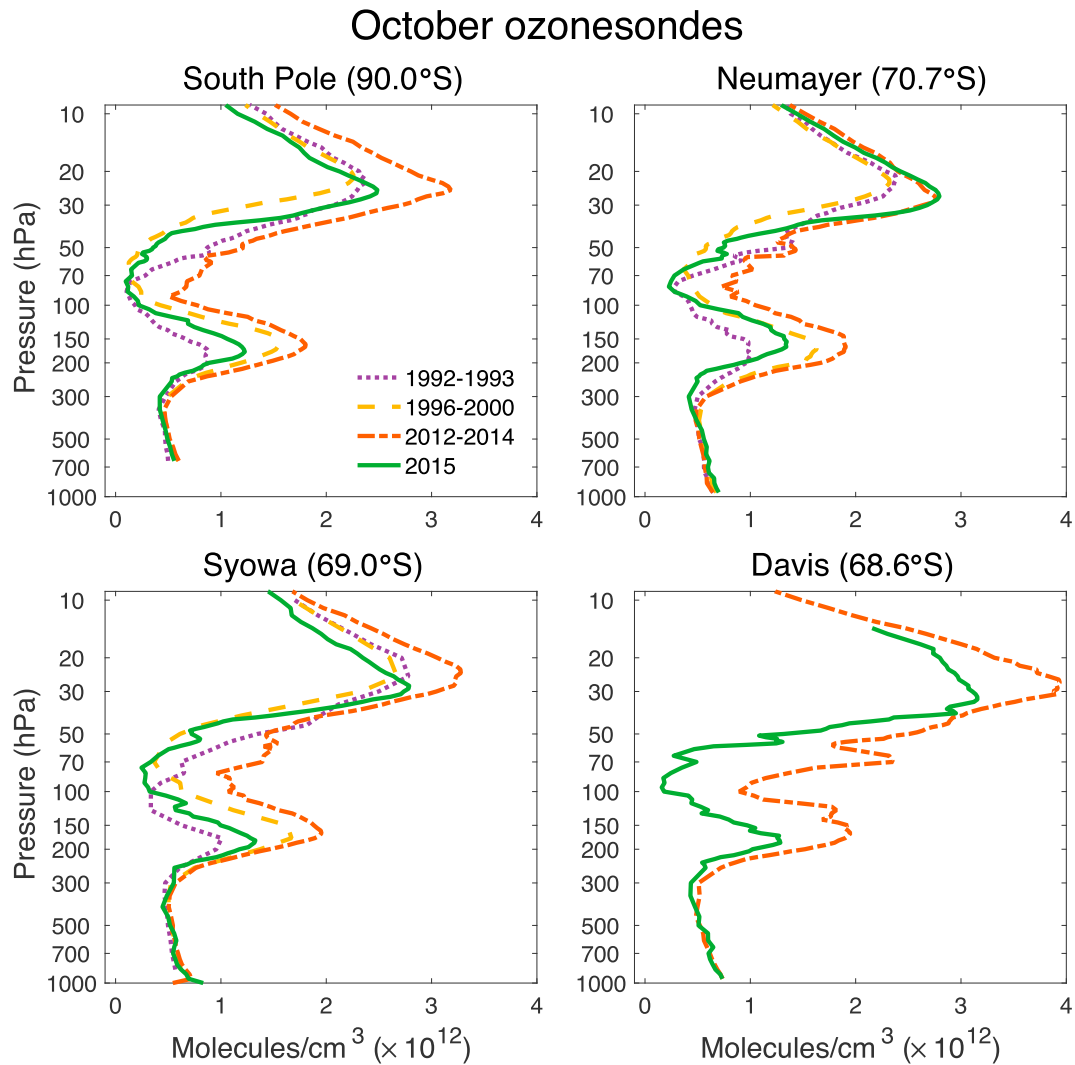


Figure 6. October averaged ozonesonde vertical profiles for the sites of South Pole, Neumayer, Syowa, and Davis. The Pinatubo volcanic period of 1992–1993 (where available) is compared against 2015 and the more volcanically clean periods of 1996–2000 and 2012–2014.

are sampled as daily average and 10° longitude by 2° latitude area average values coinciding with the ozonesonde site locations. The WACCM data are sampled as a daily average value from the closest coincident model grid box to the ozonesonde site locations. Presenting the data in this way gives the benefit of identifying and quantifying any individually low ozone observations that occurred in 2015, which can then be compared to the MAM and VC-MAM simulations.

From a qualitative point of view, examining ozonesonde time series alone without comparing against the other data sets, Figures 7 and 8 show a vast difference in ozone depletion during October and November 2015 compared to most other years in the previous decades where data are available. During October, this is especially striking for ozonesonde values at Syowa and South Pole, which show the lowest individual observations since the Pinatubo perturbed years 1992–1993. During November, exceptionally low ozone values are occurring at Davis and Neumayer, with a Neumayer measurement showing a lower value than the Pinatubo years of 1992–1993. This high-resolution ozonesonde data support the conclusion that lower stratospheric Antarctic ozone during October and November of 2015 was anomalously low.

Comparing ozonesondes with MLS and the MAM simulation shows general agreement in October and November ozone values throughout 1999–2015, albeit with some overestimation of ozone values over the entire time series, mostly in November. MAM also somewhat overestimates the depletion during the

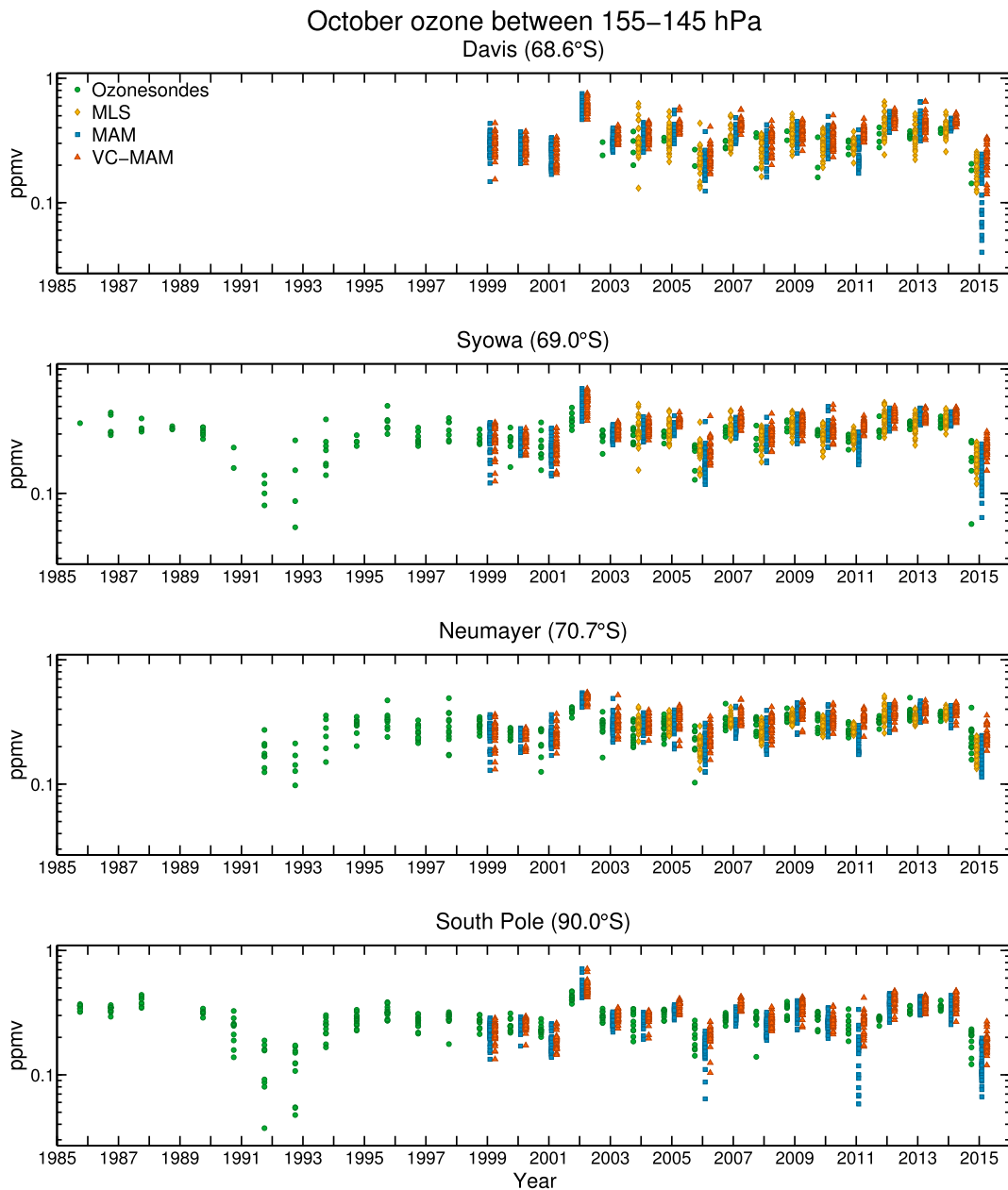


Figure 7. Individual October ozonesonde soundings averaged between 155 and 145 hPa compared to MLS, WACCM MAM, and VC-MAM daily average values at 150 hPa.

volcanic years of 2011 and 2015. Comparing MAM against VC-MAM during 2015, MAM simulates considerably lower ozone values at all sites. This occurs even though VC-MAM is also simulating very low ozone values during 2015 due to it being an abnormally cold year (see Figure S2). This indicates that within the model, aerosols are having a large influence on ozone depletion at 150 hPa that is unprecedented in 2015 compared to 1999–2014. The closest parallel is October 2011 at the South Pole, when the Puyehue-Cordón Caulle volcanic eruption (Mills et al., 2016) coincided with an abnormally cold year (Klekociuk et al., 2013). Ozonesonde and MLS values during October 2015 agree very well with MAM at Syowa and Neumayer, with a Syowa ozonesonde value the lowest from all data sets. However, at Davis and South Pole, the ozonesondes do not lie outside the VC-MAM range of values. In contrast, during November, there is strong agreement with MAM at Syowa, Neumayer, and especially Davis, where MAM, ozonesondes and MLS show the largest number of low ozone outliers. Since in some cases ozonesondes

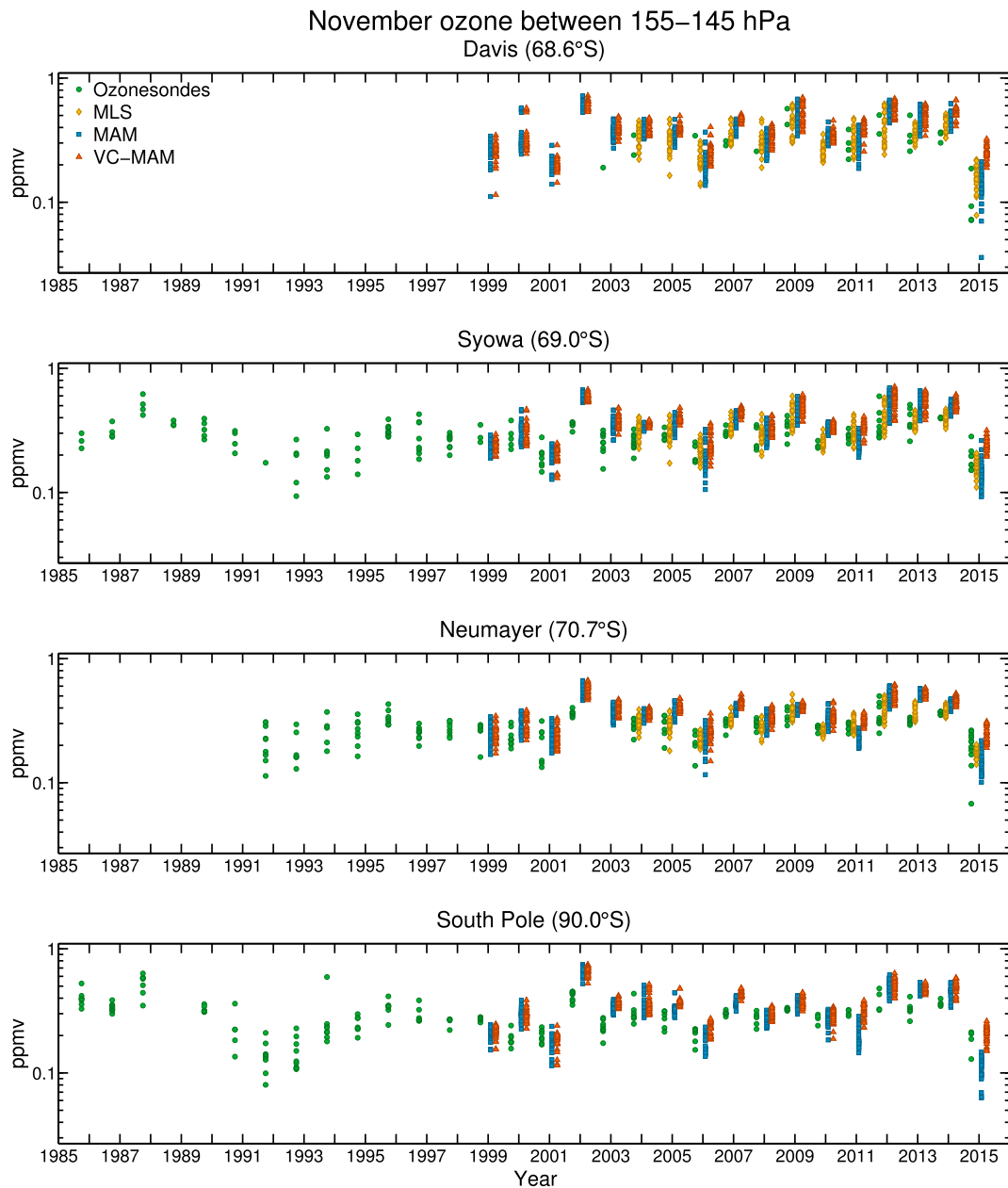


Figure 8. Same as in Figure 7 for November.

do not lie outside the VC-MAM range of values, MAM is likely slightly overestimating the influence of aerosols, mainly during October, at 150 hPa. However, due to the limited number of ozonesonde samples, the lowest values simulated by MAM are not always captured to the same extent.

The agreement between observations and MAM is slightly offset by the positive ozone bias in MAM and VC-MAM. However, the agreement between MAM and MLS in Figures 3 and 5, and the extent of the depletion seen in ozonesondes and MLS, especially at Davis, Syowa, and Neumayer, which lie in the zonal region where the largest normalized anomalies are occurring, gives confidence that the Calbuco volcanic aerosols are having a large effect on ozone levels. During October, the cold year of 2006 also shows differences between MAM and VC-MAM, albeit smaller than those of the more volcanically perturbed years of 2011 and 2015.

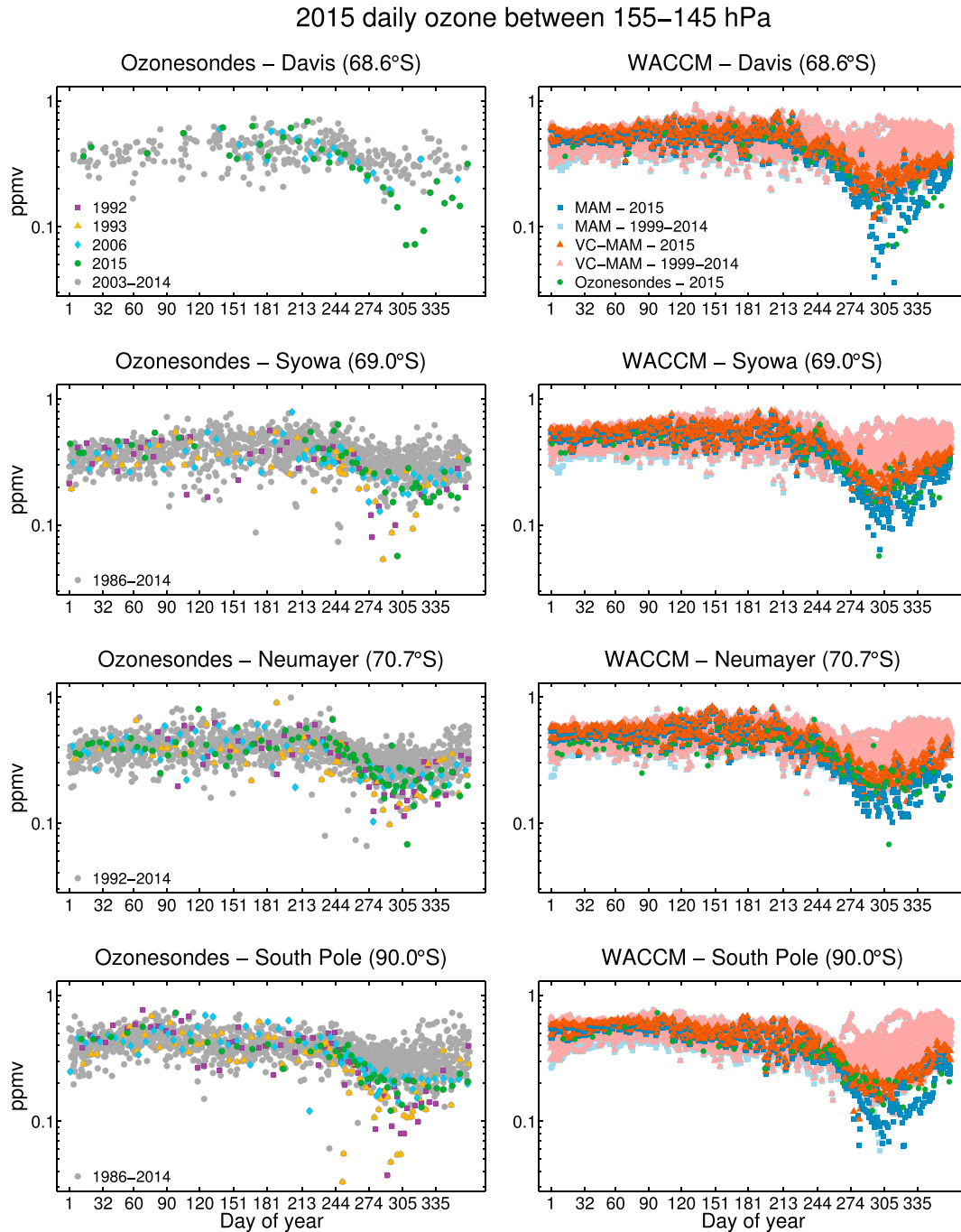


Figure 9. (left) Ozonesonde data averaged between 155 and 145 hPa and (right) MAM and VC-MAM daily averaged values from their closest coincident model grid boxes at 150 hPa plotted at their measured or simulated day of year. The ozonesonde measurements compare the large volcanically perturbed 1992 and 1993 Pinatubo years against 2015 and 2006, while the ozonesonde, MAM, and VC-MAM simulations are separately compared against each other for 2015.

The record ozone hole area that occurred in 2015 was seen largely in October. However, the ozone hole area was also at a record size through much of November and December (see Solomon et al., 2016). This indicates that the Calbuco aerosols affected the temporal evolution of the entire 2015 ozone hole season. The temporal evolution at 150 hPa is examined in Figure 9, which shows ozonesondes, MAM, and VC-MAM ozone concentrations as a function of the day of year. This gives a complementary perspective of how MAM compares to ozonesondes and how ozone depletion progressed on a daily time scale. Here ozonesonde, MAM,

and VC-MAM climatologies are shown as background values and compared to 2015 ozonesondes with the Pinatubo perturbed years of 1992 and 1993, as well as the low ozone year of 2006.

The very low Pinatubo induced ozone perturbation in 1992 and 1993 started as early as September at the South Pole and early October for Neumayer and Syowa. Ozone concentrations during the Pinatubo years stayed consistently low through the end of November for South Pole, Neumayer, and Syowa. The depletion in 2015, although not as large as 1992 and 1993, also stayed consistently low through the end of December at all stations compared to their respective climatologies. This is especially noticeable at Neumayer, Syowa, and Davis, with consistent very low ozone concentrations measured from late October to December. It is also different from 2006, with consistently lower ozone values in November and December at Syowa, Davis, and the South Pole.

Comparing MAM with VC-MAM, the major separation between the two simulations occurs in September, with peak separation occurring in late October at all ozonesonde sites. This is consistent with the very low values seen during late October through November in the ozonesonde measurements at Davis and Syowa. Coupled with the position of Syowa and especially Davis in the vortex at that time (Figure 5), and that the MAM and VC-MAM simulations remain separated until the end of 2015, there is strong evidence that the very low ozonesonde values recorded were influenced by the Calbuco volcanic aerosols.

In summary, the WACCM MAM and VC-MAM comparisons with observations in Figures 7–9 give a compelling representation of how the Calbuco volcanic aerosols influenced ozone levels, and show how consistently low the ozone levels were in 2015 compared to nearly all previous years. This is especially the case when comparing to the Pinatubo perturbed years of 1992–1993, with some 2015 values showing similar concentrations. However, it should be emphasized that the separation between MAM and VC-MAM is overestimated in some months and locations compared to the data, indicating that the model somewhat overestimates the volcanic induced loss. Nevertheless, overall this analysis indicates that, in 2015, Calbuco volcanic aerosols are having a large influence on ozone depletion, especially at the lower latitude sites, consistent with Figures 1, 3, 4, and 5.

5. Conclusions

To analyze the extent of the 2015 Calbuco volcanic eruption's influence on Antarctic ozone depletion, observations from satellite instruments and balloon-borne ozonesondes were used in combination with model simulations using a specified dynamics version of CESM1 (WACCM) model with a prognostic modal representation of stratospheric sulfate aerosol (MAM).

To track the southward progress of Calbuco aerosols, 532 nm backscatter data from CALIOP observations were compared to MAM results. After masking supercooled ternary solution and ice polar stratospheric clouds from the observed backscatter data and simulated extinction data, and applying the required scaling factors, large backscatter coefficients resulting from liquid binary sulfate were seen to extend to 68°S during October and November at 100 and 146.8 hPa, supplying additional surfaces for heterogeneous chemistry to take place. The modeled distribution and temporal spread of the Calbuco aerosols agreed well with the CALIOP data.

Additionally, although there is a significant difference in the amount of SO₂ Calbuco injected into the stratosphere (0.4 Tg) (Nicarnica Aviation, 2015; Pardini et al., 2017), compared to the Pinatubo eruption (14–23 Tg) (Guo et al., 2004), comparisons of model-derived SAD between the Pinatubo years of 1991–1993 and the Calbuco year of 2015 at 60°S and 100 hPa show similar values. This suggests that the location of the eruption is an important factor regarding the influence of volcanic aerosols in the stratosphere.

Previous studies have shown large aerosol-induced ozone depletion in the South Polar region in the years following the Pinatubo eruption (Rosenfield et al., 1997; Rozanov et al., 2002). Here we show that Calbuco aerosols also had a profound effect on ozone depletion at high southern latitudes, similar to the Pinatubo event. Through the use of normalized ozone anomalies of the 2004–2015 time series, it is shown that at 100 hPa, the largest observed excess 2015 ozone depletion occurred at latitudes between about 55 and 70°S from October to December, with the peak negative anomalies occurring in October, in broad agreement with MAM and substantially different from VC-MAM. This was similar in TCO normalized ozone anomalies; however, the difference between OMI and MAM compared to VC-MAM was not seen to the same extent as at 100 hPa. The TCO difference between MAM and VC-MAM is likely not as pronounced, since the

majority of ozone resides between 100 and 50 hPa under normal conditions, a region where volcanic aerosols will have a smaller relative influence compared to the typical PSC loadings. However, the importance of the cold stratospheric temperatures cannot be ignored, as seen in VC-MAM, with MAM exacerbating the depletion under these ideal conditions (see Ivy et al., 2017).

Substantial positive normalized ozone anomalies were observed in the southern midlatitudes in the months immediately following the eruption. This raises the question as to whether the enhanced volcanic aerosol induced an increase in transport, similar to the months following Pinatubo (Aquila et al., 2013; Poberaj et al., 2011).

Analyzing the volcanic influence in the simulations alone by subtracting VC-MAM from MAM, the volcanic aerosols are having the largest absolute effect near 65°S in both TCO and at 100 hPa during September and October of 2015. However, it is noteworthy that volcanic aerosols are affecting the entire southern mid-latitude and polar regions, with differences of 1–2% in TCO and up to 16% at 100 hPa occurring as far north as 32°S in 2015.

Due to the peak anomalies residing at latitudes lower than 70°S, the effect that volcanoes had on the expansion of the ozone hole was investigated by examining the areal size of the 220 DU contour lines for TCO and 0.275 ppmv contour lines for the 100 and 146.8 hPa levels. Due to cold dynamical conditions, the ozone hole was much larger in 2015 compared to the 2004–2014 average from September to November. As the ozone hole is typically offset from the geographical South Pole, the largest dynamical expansion compared to the 2004–2014 average occurred in the opposite direction, making the ozone hole more symmetrical about the geographic South Pole. It was also found that the presence of excess volcanic aerosols increased the size of the ozone hole by 4.4×10^6 km² (approximately 24%) in September, 3.5×10^6 km² (approximately 17%) in October, and 2.8×10^6 km² (approximately 16%) in November, with excellent agreement between MAM and OMI (as noted in Solomon et al. (2016)). At the pressure levels of 146.8 and 100 hPa, the volcanic influence was also evident in the 0.275 ppmv MLS contours. There is considerably more area displaying values below 0.275 ppmv in MAM compared to VC-MAM during October and November, with excellent agreement compared to MLS. This suggests that volcanic aerosols are acting to destroy ozone at lower latitudes. However, when comparing against the MLS 2004–2014 average, it is also seen that the dynamical and thermal conditions are indeed a significant contributor, especially closer to the South Pole.

Turning toward higher-resolution ozonesonde data, the Pinatubo years 1992–1993 and Calbuco year 2015 from the Davis, Syowa, Neumayer, and South Pole ozonesonde sites were compared with the more volcanically clean periods of 1996–2000 and 2012–2014. This suggested that volcanic aerosols had an influence on ozone depletion during 2015, especially at pressures greater than 100 hPa, where the depletion was similar to what was seen after Pinatubo in 1992–1993. Unusually low ozone was observed at the lower latitude sites of Davis and Syowa, which reside in the region of large ozone hole growth during 2015, as seen in Figure 5.

Investigating 150 hPa ozonesonde and MLS observations at the four Antarctic ozonesonde sites of South Pole, Neumayer, Syowa, and Davis again shows that some individual ozone measurements are extraordinarily low during 2015, on par with (Davis and Syowa), or even lower than (Neumayer) that observed following the 1991 eruption of Mount Pinatubo. Plots of measured ozone versus day of year show that the very low ozone levels manifested during late October and persisted through December at 150 hPa, with values consistently lower during November and December compared to other years, including cold ones (such as 2006). The MAM and VC-MAM simulations indicate that the dynamical conditions of 2015 played a significant role in these abnormal ozone depletion values, with excess volcanic aerosols further intensifying the depletion.

The excess depletion at greater pressure agrees well with previous literature that increases in volcanic aerosol can expand the typical vertical range of ozone depletion during austral spring (e.g., Hofmann & Oltmans, 1993; Hofmann et al., 1997; Solomon et al., 2005).

In summary, this analysis indicates that under the already cold and therefore ideal dynamical conditions in 2015, excess aerosols in the stratosphere from the moderate-magnitude eruption of Calbuco led to unprecedented ozone depletion. This is most noticeable at lower latitudes, where LBS aerosols can have a larger relative influence compared to deep in the vortex, acting to significantly expand the ozone hole.

The excess ozone depletion was most noticeable during late October and November, but extended through the end of 2015 based upon MLS and ozonesonde data, and their comparisons to the simulations.

Acknowledgments

Douglas E. Kinnison and Susan Solomon were supported by National Science Foundation (NSF) Frontiers in Earth System Dynamics grant OCE-1338814. WACCM is a component of the Community Earth System Model (CESM), which is supported by the National Science Foundation. Computing resources (ark:/85065/d7wd3xhc) were provided by the Climate Simulation Laboratory at National Center for Atmospheric Research (NCAR)'s Computational and Information Systems Laboratory, sponsored by the National Science Foundation and other agencies. Simulations were carried out on the Yellowstone high-performance computer platform (Computational and Information Systems Laboratory, 2012). The contributions of Michael Pitts, Lamont Poole, and Jean-Paul Vernier were supported by the NASA CALIPSO/CloudSat Science Team. Work at the Jet Propulsion Laboratory, California Institute of Technology, was carried out under contract with NASA. Ozonesonde data for the sites of Syowa and Davis are provided by the World Ozone and Ultraviolet Radiation Data Centre (WOUDC; woudc.org). The Davis ozonesonde data were collected under Australian Antarctic Science project 4293. Neumayer ozonesonde data are provided by the National Oceanic and Atmospheric Administration Network for the Detection of Atmospheric Composition Change (NOAA NDACC; http://www.ndsc.ncep.noaa.gov/sites/stat_reps/neumayer/). South Pole ozonesonde data are provided by the NOAA (esrl.noaa.gov/gmd/dv/spo_oz). OMI and MLS data are provided by the National Aeronautic and Space Administration (NASA; <https://disc.gsfc.nasa.gov/Aura/data-holdings>). The CALIPSO level 1 and level 2 science data products are archived and distributed by the Atmospheric Science Data Center (ASDC; <https://eosweb.larc.nasa.gov/>). Model results shown in this paper are available on request to the WACCM liaison, Michael J. Mills (mmills@ucar.edu).

References

- Aquila, V., Oman, L. D., Stolarski, R., Douglass, A. R., & Newman, P. A. (2013). The response of ozone and nitrogen dioxide to the eruption of Mt. Pinatubo at southern and northern midlatitudes. *Journal of the Atmospheric Sciences*, *70*(3), 894–900. <https://doi.org/10.1175/JAS-D-12-0143.1>
- Bluth, G. J. S., Doiron, S. D., Schnetzler, C. C., Krueger, A. J., & Walter, L. S. (1992). Global tracking of the SO₂ clouds from the June, 1991 Mount Pinatubo eruptions. *Geophysical Research Letters*, *19*(2), 151–154. <https://doi.org/10.1029/91GL02792>
- Brasseur, G., & Granier, C. (1992). Mount Pinatubo aerosols, chlorofluorocarbons, and ozone depletion. *Science*, *257*(5074), 1239–1242. <https://doi.org/10.1126/science.257.5074.1239>
- Brock, C. A., Hamill, P., Wilson, J. C., Jonsson, H. H., & Chan, K. R. (1995). Particle formation in the upper tropical troposphere—A source of nuclei for the stratospheric aerosol. *Science*, *270*(5242), 1650–1653. <https://doi.org/10.1126/science.270.5242.1650>
- Butchart, N. (2014). The Brewer-Dobson circulation. *Reviews of Geophysics*, *52*(2), 157–184. <https://doi.org/10.1002/2013RG000448>
- Castruccio, A., Clavero, J., Segura, A., Samaniego, P., Roche, O., Le Pennec, J. L., & Droguett, B. (2016). Eruptive parameters and dynamics of the April 2015 sub-Plinian eruptions of Calbuco volcano (southern Chile). *Bulletin of Volcanology*, *78*(9). <https://doi.org/10.1007/s00445-016-1058-8>
- Chubachi, S. (1985). A special ozone observation at Syowa station, Antarctica, from February 1982 to January 1983. In *Atmospheric Ozone* (Chap. 4, pp. 285–289). Dordrecht, Netherlands: Springer. <https://doi.org/10.1007/978-94-009-5313-0>
- Computational and Information Systems Laboratory (2012). Yellowstone: IBM iDataPlex system (Climate Simulation Laboratory). Boulder, CO: National Center for Atmospheric Research. <http://n2t.net/ark:/85065/d7wd3xhc>
- Cox, R. A., MacKenzie, A. R., Müller, R. H., Peter, Th., & Crutzen, P. J. (1994). Activation of stratospheric chlorine by reactions in liquid sulphuric acid. *Geophysical Research Letters*, *21*(13), 1439–1442. <https://doi.org/10.1029/93GL03073>
- Deshler, T., Mercer, J. L., Smit, H. G. J., Stubi, R., Levrat, G., Johnson, B. J., ... Sasaki, T. (2008). Atmospheric comparison of electrochemical cell ozonesondes from different manufacturers, and with different cathode solution strengths: The balloon experiment on standards for ozonesondes. *Journal of Geophysical Research*, *113*, D04307. <https://doi.org/10.1029/2007JD008975>
- Deshler, T., Stubi, R., Schmidlin, F. J., Mercer, J. L., Smit, H. G. J., Johnson, B. J., ... Nardi, B. (2017). Methods to homogenize electrochemical concentration cell (ECC) ozonesonde measurements across changes in sensing solution concentration or ozonesonde manufacturer. *Atmospheric Measurement Techniques*, *10*(6), 2021–2043. <https://doi.org/10.5194/amt-10-2021-2017>
- Farman, J. C., Gardiner, B. G., & Shanklin, J. D. (1985). Large losses of total ozone in Antarctica reveal seasonal ClO_x/NO_x interaction. *Nature*, *315*(6016), 207–210. <https://doi.org/10.1038/315207a0>
- Guo, S., Bluth, G. J. S., Rose, W. I., Watson, I. M., & Prata, A. J. (2004). Re-evaluation of SO₂ release of the 15 June 1991 Pinatubo eruption using ultraviolet and infrared satellite sensors. *Geochemistry, Geophysics, Geosystems*, *5*, Q04001. <https://doi.org/10.1029/2003GC000654>
- Hanson, D. R., Ravishankara, A. R., & Solomon, S. (1994). Heterogeneous reactions in sulfuric acid aerosols: A framework for model calculations. *Journal of Geophysical Research*, *99*(D2), 3615–3629. <https://doi.org/10.1029/93JD02932>
- Hofmann, D. J., Oltmans, S. J., Harris, J. M., Johnson, B. J., & Lathrop, J. A. (1997). Ten years of ozonesonde measurements at the South Pole: Implications for recovery of springtime Antarctic ozone. *Journal of Geophysical Research*, *102*(12), 8931–8943. <https://doi.org/10.1029/2005GL025232>
- Hofmann, D. J., & Oltmans, S. J. (1993). Anomalous Antarctic ozone during 1992: Evidence for Pinatubo volcanic aerosol effects. *Journal of Geophysical Research*, *98*(D10), 18,555–18,561. <https://doi.org/10.1029/93JD02092>
- Hofmann, D. J., Oltmans, S. J., Harris, J. M., Solomon, S., Deshler, T., & Johnson, B. J. (1992). Observations and possible causes of new ozone depletion in Antarctica in 1991. *Nature*, *355*(6357), 242–244. <https://doi.org/10.1038/355242a0>
- Hofmann, D. J., & Solomon, S. (1989). Ozone destruction through heterogeneous chemistry following the eruption of El Chichón. *Journal of Geophysical Research*, *94*(D4), 5029–5041. <https://doi.org/10.1029/JD094iD04p05029>
- Ivy, D. J., Solomon, S., Kinnison, D., Mills, M. J., Schmidt, A., & Neely III, R. R. (2017). The influence of the Calbuco eruption on the 2015 Antarctic ozone hole in a fully coupled chemistry-climate model. *Geophysical Research Letters*, *44*, 2556–2561. <https://doi.org/10.1002/2016GL071925>
- Jäger, H., & Deshler, T. (2002). Lidar backscatter to extinction, mass and area conversions for stratospheric aerosols based on midlatitude balloonborne size distribution measurements. *Geophysical Research Letters*, *29*(7), 1929. <https://doi.org/10.1029/2003GL017189>
- Jäger, H., & Deshler, T. (2003). Correction to "Lidar backscatter to extinction, mass and area conversions for stratospheric aerosols based on midlatitude balloonborne size distribution measurements". *Geophysical Research Letters*, *30*(7), 1382. <https://doi.org/10.1029/2003GL017189>
- Junge, C. E., Chagnon, C. W., & Manson, J. E. (1961). A world-wide stratospheric aerosol layer. *Science*, *133*(3463), 1478–1479. <https://doi.org/10.1126/science.133.3463.1478-a>
- Kinnison, D. E., Brasseur, G. P., Walters, S., Garcia, R. R., Marsh, D. R., Sassi, F., ... Simmons, A. J. (2007). Sensitivity of chemical tracers to meteorological parameters in the MOZART-3 chemical transport model. *Journal of Geophysical Research*, *112*, D20302. <https://doi.org/10.1029/2006JD007879>
- Klekociuk, A. R., Tully, M. B., Krummel, P. B., Gies, H. P., Petelina, S. V., Alexander, S. P., ... Stone, K. A. (2013). The Antarctic ozone hole during 2011. *Australian Meteorological and Oceanographic Journal*, *64*, 293–311.
- Kremser, S., Thomason, L. W., von Hobe, M., Hermann, M., Deshler, T., Timmreck, C., ... Meland, B. (2016). Stratospheric aerosol—Observations, processes and impact on climate. *Reviews of Geophysics*, *54*(2), 278–335. <https://doi.org/10.1002/2015RG000511>
- Levelt, P. F., Hilsenrath, E., Leppelmeier, G. W., van den Oord, G. H. J., Bhartia, P. K., Tamminen, J., ... Veefkind, J. P. (2006). Science objectives of the ozone monitoring instrument. *IEEE Transactions on Geoscience and Remote Sensing*, *44*(5), 1199–1208. <https://doi.org/10.1109/TGRS.2006.872336>
- Livesey, N. J., Read, W. G., Wagner, P. A., Froidevaux, L., Lambert, A., Manney, G. L., ... Knosp, B. W. (2016). Version 4.2x level 2 data quality and description document D-33509. Pasadena, CA: Jet Propulsion Laboratory, California Institute of Technology.
- Marsh, D. R., Mills, M. J., Kinnison, D. E., Lamarque, J.-F., Calvo, N., & Polvani, L. M. (2013). Climate change from 1850 to 2005 simulated in CESM1 (WACCM). *Journal of Climate*, *26*(19), 7372–7391. <https://doi.org/10.1175/JCLI-D-12-00558.1>

- McPeters, R. D., Bhartia, P. K., Krueger, A. J., Herman, J. R., Wellemeyer, C. G., Seftor, C. J., ... Cebula, R. P. (1998). Earth Probe Total Ozone Mapping Spectrometer (TOMS) data product user's guide.
- Mills, M. J., Schmidt, A., Easter, R., Solomon, S., Kinnison, D. E., Ghan, S. J., ... Gettelman, A. (2016). Global volcanic aerosol properties derived from emissions, 1990–2014, using CESM1 (WACCM). *Journal of Geophysical Research: Atmospheres*, *121*, 2332–2348. <https://doi.org/10.1002/2015JD024290>
- Molina, M. J., Zhang, R., Wooldridge, P. J., McMahon, J. R., Kim, J. E., Chang, H. Y., & Beyer, K. D. (1993). Physical chemistry of the H₂SO₄/HNO₃/H₂O system: Implications for polar stratospheric clouds. *Science*, *261*(5127), 1418–1423. <https://doi.org/10.1126/science.261.5127.1418>
- Neely III, R.R., & Schmidt, A. (2016). VolcanEESM: Global volcanic sulphur dioxide (SO₂) emissions database from 1850 to present—Version 1.0. Centre for Environmental Data Analysis, 04 February 2016. <https://doi.org/10.5285/76ebdc0b-0eed-4f70-b89e-55e606bcd568>
- Newman, P. A., Kawa, S. R., & Nash, E. R. (2004). On the size of the Antarctic ozone hole. *Geophysical Research Letters*, *31*, L21104. <https://doi.org/10.1029/2004GL020596>
- Nicarica Aviation (2015). Calbuco eruption, April 2015: AIRS satellite measurements. Retrieved from <http://nicaricaaviation.com/calbuco-eruption-april-2015/>
- Pardini, F., Burton, M., Arzilli, F., La Spina, G., & Polacci, M. (2017). Satellite-derived SO₂ flux time-series and magmatic processes during the 2015 Calbuco eruptions. *Solid Earth Discussions*, 1–25. <https://doi.org/10.5194/se-2017-64>
- Pitts, M. C., Poole, L. R., Lambert, A., & Thomason, L. W. (2013). An assessment of CALIOP polar stratospheric cloud composition classification. *Atmospheric Chemistry and Physics*, *13*(6), 2975–2988. <https://doi.org/10.5194/acp-13-2975-2013>
- Pitts, M. C., Poole, L. R., & Thomason, L. W. (2009). CALIPSO polar stratospheric cloud observations: Second-generation detection algorithm and composition discrimination. *Atmospheric Chemistry and Physics*, *9*(19), 7577–7589. <https://doi.org/10.5194/acp-9-7577-2009>
- Poberaj, C. S., Staehelin, J., & Brunner, D. (2011). Missing stratospheric ozone decrease at southern hemisphere middle latitudes after Mt. Pinatubo: A dynamical perspective. *Journal of the Atmospheric Sciences*, *68*(9), 1922–1945. <https://doi.org/10.1175/JAS-D-10-05004.1>
- Portmann, R. W., Solomon, S., Garcia, R. R., Thomason, L. W., Poole, L. R., & McCormick, M. P. (1996). Role of aerosol variations in anthropogenic ozone depletion in the polar regions. *Journal of Geophysical Research*, *101*(D17), 22,991–23,006. <https://doi.org/10.1029/96JD02608>
- Rienecker, M. M., Suarez, M. J., Gelaro, R., Todling, R., Bacmeister, J., Liu, E., ... Woollen, J. (2011). MERRA: NASA's Modern-Era Retrospective Analysis for Research and Applications. *Journal of Climate*, *24*(14), 3624–3648. <https://doi.org/10.1175/JCLI-D-11-00015.1>
- Rogers, R. R., Hostetler, C. A., Hair, J. W., Ferrare, R. A., Liu, Z., Obland, M. D., ... Winker, D. M. (2011). Assessment of the CALIPSO lidar 532 nm attenuated backscatter calibration using the NASA LaRC airborne high spectral resolution lidar. *Atmospheric Chemistry and Physics*, *11*(3), 1295–1311. <https://doi.org/10.5194/acp-11-1295-2011>
- Romero, J. E., Morgavi, D., Arzilli, F., Daga, R., Caselli, A., Reckziegel, F., ... Perugini, D. (2016). Eruption dynamics of the 22–23 April 2015 Calbuco volcano (southern Chile): Analyses of tephra fall deposits. *Journal of Volcanology and Geothermal Research*, *317*, 15–29. <https://doi.org/10.1016/j.jvolgeores.2016.02.027>
- Rosenfield, J. E., Considine, D. B., Meade, P. E., Bacmeister, J. T., Jackman, C. H., & Schoeberl, M. R. (1997). Stratospheric effects of Mount Pinatubo aerosol studied with a coupled two-dimensional model. *Journal of Geophysical Research*, *102*(D3), 3649–3670. <https://doi.org/10.1029/96JD03820>
- Rozanov, E. V., Schlesinger, M. E., Andronova, N. G., Yang, F., Malyshev, S. L., Zubov, V. A., ... Li, B. (2002). Climate/chemistry effects of the Pinatubo volcanic eruption simulated by the UIUC stratosphere/troposphere GCM with interactive photochemistry. *Journal of Geophysical Research*, *107*(D21), 4594. <https://doi.org/10.1029/2001JD000974>, ACL 12-1–ACL 12-14
- Smit, H. G. J., Straeter, W., Johnson, B. J., Oltmans, S. J., Davies, J., Tarasick, D. W., ... Posny, F. (2007). Assessment of the performance of ECC-ozonesondes under quasi-flight conditions in the environmental simulation chamber: Insights from the Juelich Ozone Sonde Intercomparison Experiment (JOSIE). *Journal of Geophysical Research*, *112*, D19306. <https://doi.org/10.1029/2006JD007308>
- Solomon, S. (1999). Stratospheric ozone depletion: A review of concepts and history. *Reviews of Geophysics*, *37*(3), 275–316. <https://doi.org/10.1029/1999RG900008>
- Solomon, S., Daniel, J. S., Neely III, R. R., Vernier, J.-P., Dutton, E. G., & Thomason, L. W. (2011). The persistently variable “background” stratospheric aerosol layer and global climate change. *Science*, *333*(6044), 866–870. <https://doi.org/10.1126/science.1206027>
- Solomon, S., Garcia, R. R., Rowland, F. S., & Wuebbles, D. J. (1986). On the depletion of Antarctic ozone. *Nature*, *321*(6072), 755–758. <https://doi.org/10.1038/321755a0>
- Solomon, S., Ivy, D. J., Kinnison, D., Mills, M. J., Neely III, R. R., & Schmidt, A. (2016). Emergence of healing in the Antarctic ozone layer. *Science*, *353*(6296), 269–274. <https://doi.org/10.1126/science.aae0061>
- Solomon, S., Kinnison, D., Bandoro, J., & Garcia, R. (2015). Simulation of polar ozone depletion: An update. *Journal of Geophysical Research: Atmospheres*, *120*(15), 7958–7974. <https://doi.org/10.1002/2015JD023365>
- Solomon, S., Portmann, R. W., Garcia, R. R., Randel, W., Wu, F., Nagatani, R., ... McCormick, M. P. (1998). Ozone depletion at mid-latitudes: Coupling of volcanic aerosols and temperature variability to anthropogenic chlorine. *Geophysical Research Letters*, *25*(11), 1871–1874. <https://doi.org/10.1029/98GL01293>
- Solomon, S., Portmann, R. W., Garcia, R. R., Thomason, L. W., Poole, L. R., & McCormick, M. P. (1996). The role of aerosol variations in anthropogenic ozone depletion at northern midlatitudes. *Journal of Geophysical Research*, *101*(D3), 6713–6727. <https://doi.org/10.1029/95JD03353>
- Solomon, S., Portmann, R. W., Sasaki, T., Hofmann, D. J., & Thompson, D. W. J. (2005). Four decades of ozonesonde measurements over Antarctica. *Journal of Geophysical Research*, *110*, D21311. <https://doi.org/10.1029/2005JD005971>
- Tilmes, S., Müller, R., Salawitch, R. J., Schmidt, U., Webster, C. R., Oelhaf, H., ... Russell III, J. M. (2008). Chemical ozone loss in the Arctic winter 1991–1992. *Atmospheric Chemistry and Physics*, *7*(4), 10,097–10,129. <https://doi.org/10.5194/acpd-7-10097-2007>
- Vernier, J.-P., Thomason, L. W., Pommereau, J. P., Bourassa, A., Pelon, J., Garnier, A., ... Vargas, F. (2011). Major influence of tropical volcanic eruptions on the stratospheric aerosol layer during the last decade. *Geophysical Research Letters*, *38*, L12807. <https://doi.org/10.1029/2011GL047563>
- Wegner, T., Kinnison, D. E., Garcia, R. R., & Solomon, S. (2013). Simulation of polar stratospheric clouds in the specified dynamics version of the Whole Atmosphere Community Climate Model. *Journal of Geophysical Research: Atmospheres*, *118*, 4991–5002. <https://doi.org/10.1002/jgrd.50415>
- Winker, D. M., Vaughan, M. A., Omar, A., Hu, Y., Powell, K. A., Liu, Z., ... Young, S. A. (2009). Overview of the CALIPSO mission and CALIOP data processing algorithms. *Journal of Atmospheric and Oceanic Technology*, *26*(11), 2310–2323. <https://doi.org/10.1175/2009JTECHA1281.1>
- World Meteorological Organization (WMO) (2015). WMO Antarctic ozone bulletins (2015). Retrieved from www.wmo.int/pages/prog/arep/WMOAntarcticOzoneBulletins2015.html